Seventh International Conference on Computational Fluid Dynamics (ICCFD7), Big Island, Hawaii, July 9-13, 2012

ICCFD7-1903

Improvement of Two-Equation Turbulence Model with Anisotropic Eddy-Viscosity for Hybrid Rocket Research

M. Mikiro* and T. Shimada**
Corresponding author: tt107393@mail.ecc.u-tokyo.ac.jp

* Department of Aeronautics and Astronautics, School of Engineering, the University of Tokyo, Japan.
** Institute of Space and Astronautical Science, Japan Aerospace Exploration Agency.

Abstract: For a hybrid rocket engine, it has been proven by ground and flight experiments that the fuel regression rate can be accelerated by swirling injection of the oxidizer. It is known a swirling turbulent flow has anisotropic nature in its turbulent viscosity. In this study, the objective is to improve the applicability of existing treatment of isotropic turbulent model such as two-equation, eddy viscosity, model by introducing anisotropic eddy-viscosity coefficients that can adjust particular direction of these with substantial derivative of vorticity, in order to simulate swirling turbulent flows in hybrid rocket engines. Simulation results for some swirling turbulent flows with the existing model and with an improved model will be compared.

Keywords: Swirling Flow, Turbulence Modeling, RANS, Hybrid Rocket.

1 Background and Objectives

Hybrid rocket propulsion is one of space propulsion techniques for the next generation now researched actively. As shown in Figure 1, this type of rocket consists of solid fuel and liquid oxidizer. Typically, acrylic or wax is used as the solid fuel, and liquid oxygen is used as the oxidizer. Therefore, it has high safety because the fuel does not contain explosives as ingredients and low environmental load by exhaust than that of a solid rocket motor. In addition, the rocket shows good characteristics of capability that thrust modulation like a liquid rocket engine, and higher specific impulse than a solid rocket motor.

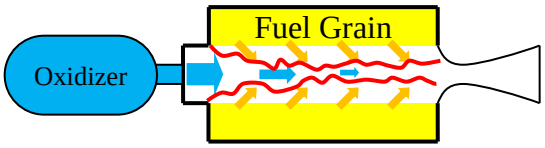

Figure 1: Outline of a hybrid rocket engine

Though, in case a conventional fuel, such as, HTPB or PE, etc., a hybrid rocket engine has limitation that only low fuel regression rate can be obtained. As one of methods for enhancing fuel regression rate, a swirling-oxidizer-typed hybrid rocket engine that induces swirling flow in the chamber was invented. It has been clarified by experimental investigations that the regression rate can be improved by this method. Also, some numerical studies are reported.

In general, for the case that CFD is employed as a design tool of the combustion chamber, the Reynolds Averaged Navier-Stokes (RANS) equations have been used because of their reasonable computational costs compared to those of LES and DNS. On this occasion, a two-equation turbulence

model, such as k - ε model, has been often selected in order to obtain turbulence stresses. However, as is well known, ordinary liner turbulence models based on the eddy-viscosity assumption cannot simulate flow field like swirling turbulence in pipe precisely. Because the turbulence transport in swirling flows is usually anisotropic which is small in selective directions, a turbulent model assuming isotropic turbulence transport cannot describe swirling flow in principle. Hence the Reynolds stress models (RSM) solving for each directional Reynolds stresses have been used for these swirling flow field. Though, because the variables of these models are increased by numbers of elements of Reynolds stresses, complexity of coding and calculation cost widely increase in comparison with standard two-equation turbulence models.

Recently, Yoshizawa, et al. have developed the improved two-equation turbulence model, which is usable for simulating swirling turbulence flow [1]·This model is based on the standard k - ε model. An eddy-viscosity of this model is reduced by a coefficient constructed with substantial derivative of vorticity indicating swirling of mean flow. So, the turbulence stresses of all directions are reduced uniformly.

Authors simulated the experiment of low velocity swirling flow in a pipe by Murakami, et al. [2] as a prior case for evaluating applicability of the improved model to the swirling-oxidizer-typed hybrid rocket engine [3]. And it was confirmed that the predictive accuracy for weak swirling flow is clearly improved than the result of standard k - ε model. Though, the result that applying improved model to strong swirling flow for instance vortex-tube was not favorable. It is considered that these flow fields have strong anisotropic turbulence. Hence, authors attempt to that improvement simulation result of Yoshizawa model by adding nonlinear term of turbulent stress formulation of helicity model in order to append property of anisotropy to eddy viscosity. Objective of this study is to comprehend characteristic of this model by means of simulate existing experimental results and to validate availability.

2 Governing Equations

Favre averaged turbulent compressible Navier-Stokes Equations are used as governing equations, which are written in terms of mean variables as follows.

Mass conservation:

$$\frac{\partial \rho}{\partial t}+\frac{\partial}{\partial x_j}\left(\rho u_j\right)=0 \tag{1}$$

Momentum conservation:

$$\frac{\partial}{\partial t}\left(\rho u_i\right)+\frac{\partial}{\partial x_j}\left(\rho u_j u_i\right)=-\frac{\partial p}{\partial x_i}+\frac{\hat{\tau}_{ji}}{\partial x_j} \tag{2}$$

Mean energy conservation:

$$\frac{\partial}{\partial t}\left(\rho E\right)+\frac{\partial}{\partial x_j}\left(\rho u_j H\right)=\frac{\partial}{\partial x_j}\left[u_i\hat{\tau}_{ij}+\left(\mu+\frac{\mu_t}{\sigma_k}\right)\frac{\partial k}{\partial x_j}-q_j\right] \tag{3}$$

And where,

$$\hat{\tau}_{ij}=2\mu\left[S_{ij}-\frac{1}{3}\frac{\partial u_k}{\partial x_k}\delta_{ij}\right]+R_{ij} \tag{4}$$

$$S_{ij}=\left(\frac{\partial u_i}{\partial x_j}+\frac{\partial u_j}{\partial x_i}\right) \tag{5}$$

$$E=e+\frac{1}{2}u_i u_i+k=h-\frac{p}{\rho}+\frac{1}{2}u_i u_i+k \tag{6}$$

$$q_j=-Cp\left(\frac{\mu}{\mathrm{Pr}_L}+\frac{\mu_T}{\mathrm{Pr}_T}\right)\frac{\partial T}{\partial x_j} \tag{7}$$

and t is time, x_i is cartesian coordinate, i and j are suffix, ρ is density, u_i is velocity component, p is pressure, E is specific total energy, H is specific total enthalpy, k is turbulence energy, S_{ij} is stress tensor, T is temperature, q_i is heat flux, Cp is constant pressure specific heat, Pr_L is laminar Prantdtl number and Pr_T is turbulent Prantdtl number. Definition of unit mass enthalpy $h = e + p/\rho$ and an equation of state $p = \rho RT$ are added to the above equation system with specific internal energy e and gas constant R. The eddy viscosity μ_t and the turbulent strain tensor R_{ij} are evaluated by turbulence model.

3 Turbulence Models

The composite time scale k-ε model (hereinafter called Yoshizawa model) build by Yoshizawa et al. [1] is shown below, which is base turbulence model of current study. In case of normal two equations turbulence model, turbulence energy cascade time scale τ_E is often used to determine eddy viscosity. The characteristic of this composite time scale model is to use time scale of strain τ_S, time scale of vorticity τ_Ω and time scale of lagrangian variation of vorticity vector in addition to τ_E. Formulations of these time scales are shown as follows.

$$\tau_S = \frac{1}{\sqrt{S_{ij}{}^2}} \tag{8}$$

$$\tau_\Omega = \frac{1}{\sqrt{\Omega_{ij}{}^2}} \tag{9}$$

$$\tau_L = 1 \Bigg/ \left(\left(\frac{D\boldsymbol{\Omega}}{Dt} \right)^2 \right)^{1/4} \tag{10}$$

And Ω_{ij} is vorticity tensor and $\boldsymbol{\Omega}$ is vorticity vector.

These time-scale-effects are incorporated as correction factor Λ in production of eddy viscosity μ_t with conventional formulation used in normal k-ε model. Formulations of this turbulence model are shown as follows.

Turbulent energy transport:

$$\frac{\partial(\rho k)}{\partial t} + \frac{\partial(\rho u_j k)}{\partial x_j} = R_{ij}\frac{\partial u_i}{\partial x_j} - \rho\varepsilon + \frac{\partial}{\partial x_j}\left[\left(\mu + \frac{\mu_t}{\sigma_k} \right) \frac{\partial k}{\partial x_j} \right] \tag{11}$$

Turbulent energy dissipation rate transport:

$$\frac{\partial(\rho\varepsilon)}{\partial t} + \frac{\partial(\rho u_j \varepsilon)}{\partial x_j} = C_{\varepsilon 1}\frac{\varepsilon}{k}R_{ij}\frac{\partial u_i}{\partial x_j} - C_{\varepsilon 2} f_2 \rho \frac{\varepsilon^2}{k} + \frac{\partial}{\partial x_j}\left[\left(\mu + \frac{\mu_t}{\sigma_\varepsilon} \right) \frac{\partial \varepsilon}{\partial x_j} \right] \tag{12}$$

And where,

$$\mu_t = C_V f_1 \rho \frac{k^2/\varepsilon}{\Lambda} \tag{13}$$

$$\Lambda = \sqrt{1 + C_S\left(\frac{k}{\varepsilon} S_{ij} \right)^2 + C_{\Omega L}\left(\frac{k}{\varepsilon}\boldsymbol{\Omega} \right)^2 \left(\frac{k^2}{\varepsilon^2}\frac{D\boldsymbol{\Omega}}{Dt} \right)^2} \tag{14}$$

$$R_{ij} = 2\mu_t \left[\mathbf{S}_{ij} - \frac{1}{3}\frac{\partial u_j}{\partial x_i}\delta_{ij} \right] - \frac{2}{3}\delta_{ij}\rho k \tag{15}$$

Where, f_1 and f_2 are low-Reynolds number correction functions. In this study, the functions constructed by Abe et al.[6] are used. In this case, for the propose of steady state analysis, Lagrange derivative is defined as follows,

$$\frac{D\mathbf{\Omega}}{Dt} = u_i \frac{\partial \mathbf{\Omega}}{\partial x_i} \tag{16}$$

In addition, central difference scheme is used to discretize this derivative and the model constants are indicated as follows.

$$C_V = 0.12,\ C_S = 0.015,\ C_{\Omega L} = 0.3,\ \sigma_k = 1.4,\ \sigma_\varepsilon = 1.4,\ C_{\varepsilon 1} = 1.5,\ C_{\varepsilon 2} = 1.9$$

In the case of swirling flow, this model describes laminarization phenomenon at center of pipe due to suppress production of eddy viscosity by means of that third term of inner root of Λ become dominant and Λ is more than 1.

The k-ε-H model build by Yokoi et, al. [4] (hereinafter called helicity model) is shown below. This model consists of three transport equations of turbulent energy, dissipation rate and turbulent helicity H ($H = \mathbf{u}' \cdot \boldsymbol{\omega}'$) which describe swirling of turbulence in flow and turbulent stress tensor is nonlinear.

Turbulent energy transport:

$$\frac{\partial(\rho k)}{\partial t} + \frac{\partial(\rho u_j k)}{\partial x_j} = R_{ij}\frac{\partial u_i}{\partial x_j} - \rho\varepsilon + \frac{\partial}{\partial x_j}\left[\left(\mu + \frac{\mu_t}{\sigma_k} \right) \frac{\partial k}{\partial x_j} \right] \tag{17}$$

Turbulent energy dissipation rate transport:

$$\frac{\partial(\rho\varepsilon)}{\partial t} + \frac{\partial(\rho u_j \varepsilon)}{\partial x_j} = C_{\varepsilon 1}\frac{\varepsilon}{k}R_{ij}\frac{\partial u_i}{\partial x_j} - C_{\varepsilon 2} f_2 \rho \frac{\varepsilon^2}{k} - C_{\varepsilon 3}\frac{k^2}{\varepsilon}\mathbf{\Omega}\cdot\nabla H + \frac{\partial}{\partial x_j}\left[\left(\mu + \frac{\mu_t}{\sigma_\varepsilon} \right) \frac{\partial \varepsilon}{\partial x_j} \right] \tag{18}$$

Turbulent helicity transport:

$$\frac{\partial(\rho H)}{\partial t} + \frac{\partial(\rho u_j H)}{\partial x_j} = R_{ij}\frac{\partial \Omega_i}{\partial x_j} - \Omega_i \frac{\partial R_{ij}}{\partial x_j} - C_{H'}\frac{\rho\varepsilon}{k}H + \frac{\partial}{\partial x_j}\left[\left(k\Omega_j + \frac{\mu_t}{\sigma_H} \right) \frac{\partial H}{\partial x_j} \right] \tag{19}$$

And where,

$$R_{ij} = 2\mu_t \left[\mathbf{S}_{ij} - \frac{1}{3}\frac{\partial u_j}{\partial x_i}\delta_{ij} \right] - \frac{2}{3}\delta_{ij}\rho k - \eta\left[\Omega_i \frac{\partial H}{\partial x_j} + \Omega_j \frac{\partial H}{\partial x_i} - \frac{2}{3}(\mathbf{\Omega}\cdot\nabla H)\delta_{ij} \right] \tag{20}$$

$$\eta = C_\eta \frac{k^4}{\varepsilon^3} \tag{21}$$

The turbulence model using in this study is composed by that adding nonlinear term of turbulent stress of helicity model to that of Yoshizawa model. Namely, equation of turbulent stress tensor of Yoshizawa model is changed from equation (15) to equation (20), and equation of dissipation rate is changed from equation (12) to equation (19) in terms of count the effect of helicity. Where, the helicity H is obtained from equation (19) under the assumption of local equilibrium as below.

$$H = \frac{1}{C_H}\frac{k}{\rho\varepsilon}\left(R_{ij}\frac{\partial \Omega_i}{\partial x_j} - \Omega_i \frac{\partial R_{ij}}{\partial x_j} \right) \tag{22}$$

Yoshizawa model is the turbulence model that has isotropic eddy viscosity, but by adding nonlinear term to turbulent stress, it can be considered that the isotropic eddy viscosity is converted into anisotropic eddy viscosity as follows.

$$R_{ij} = 2\mu_t\left[\left(\frac{\partial u_i}{\partial x_j}+\frac{\partial u_j}{\partial x_i}\right) - \frac{1}{3}\frac{\partial u_j}{\partial x_i}\delta_{ij}\right] - \frac{2}{3}\delta_{ij}\rho k - \eta\left[\Omega_i\frac{\partial H}{\partial x_j} + \Omega_j\frac{\partial H}{\partial x_i} - \frac{2}{3}(\mathbf{\Omega}\cdot\nabla H)\delta_{ij}\right] \tag{23}$$

$$R_{ij} = 2\left\{\mu_t - \eta\left[\Omega_i\frac{\partial H}{\partial x_j} + \Omega_j\frac{\partial H}{\partial x_i} - \frac{2}{3}(\mathbf{\Omega}\cdot\nabla H)\delta_{ij}\right] \Big/ 2\left[\mathbf{S}_{ij} - \frac{1}{3}\frac{\partial u_j}{\partial x_i}\delta_{ij}\right]\right\}\left[\mathbf{S}_{ij} - \frac{1}{3}\frac{\partial u_j}{\partial x_i}\delta_{ij}\right] - \frac{2}{3}\delta_{ij}\rho k \tag{24}$$

$$R_{ij} = 2\overline{\mu}_{t_{ij}}\left[\mathbf{S}_{ij} - \frac{1}{3}\frac{\partial u_j}{\partial x_i}\delta_{ij}\right] - \frac{2}{3}\delta_{ij}\rho k \tag{25}$$

The coefficients appear on Yoshizawa model are not changed, and that appear on helicity model are shown as follows, which are set with experimentally trial calculations.

$$C_\eta = 1\times10^{-6},\ \ C_{\varepsilon 3} = 1\times10^{-4},\ \frac{1}{C_H} = 1\times10^{-2}$$

4 Numerical Method

The governing equations are specially discretized by finite volume method. Numerical flux of convection term is calculated due to SLAU scheme constructed by Shima et al. [5] The 3rd order MUSCL scheme regulated by Van-Albada slope limiter with primitive variable interpolation is used to obtain higher order accuracy at cell boundary. Numerical flux of viscous term is evaluated by 2nd order central difference scheme. 2nd order 2 stages Runge-Kutta scheme is used to integrate time derivative term.

5 Numerical Setup

Two case of swirling flow are selected as analysis objects. One case is an experiment conducted by Murakami et, al. which has retard flow in center of the pipe and use water as working fluid. Another is an experiment by Kito [6] which indicate strong reverse flow in center and use air as working fluid. The numerical grid point number for the former case is about 0.3 million, and the number of each directions of axial, radius and circumferential are 71, 51 and 81 points respectively, and the grid number for the latter case is about 0.58 million, and the number of each directions are 101, 71 and 81 points respectively. The minimum grid length is about 10 μm at wall in each case. The velocity boundary conditions of axial and circumferential direction at inlet are adopted velocity profiles which were measured by experiment, and radius direction velocity set to "0". In case of experiment of Murakami et, al., the position measuring velocity is at distance of 50 times of pipe radius R_0 from the swirler, and in case of Kito et, al., the position is 10.4 times of pipe radius R_0. Because the data of velocity profile have been nondimensionalized by bulk velocity, in this study, the bulk velocity is set to 5 m/s. In this case, the Reynolds number is about order of 10^5. The free outflow condition is imported at outlet boundary and the non-slip condition is set at the wall. The boundary conditions for

k and ε are shown below, where, suffix “in” and “w” indicate “inflow” and “wall”, respectively.

Inflow Condition:

$$k_{in} = 0.002 \times U_m^{\,2} \tag{26}$$

$$\varepsilon_{in} = 0.09 \times k^{2/3} / (0.1 \times R_0) \tag{27}$$

Wall Condition:

$$k_w = 0 \tag{28}$$

$$\varepsilon_w = 2 \frac{\mu}{\rho} \left[\frac{\partial \sqrt{k}}{\partial n} \right]_w^2 \tag{29}$$

6 Results and Discussion

First, the simulation results for the experiment by Murakami et, al. are shown. Figure 2 and Figure 3 indicate radial distribution of axial velocity and circumferential velocity, respectively, both of them are averaged circumferentially and are nondimensionalized. In both figures, dot indicates the experimental values, dashed line and solid line indicate position of measuring sections which are 14 R_0 and 17.8 R_0 from inlet, line color of red and blue indicate current model and Yoshizawa model, respectively.

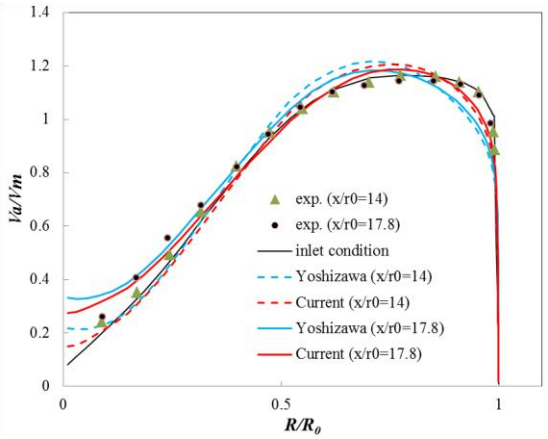

Figure 2: Axial velocity distributions

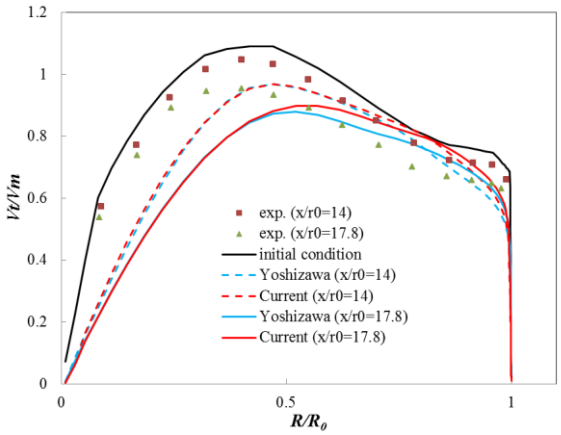

Figure 3: Circumferential velocity distributions

In Figure 2, about axial velocity distribution, it can be seen that the current model simulate better results than that of the Yoshizawa model in central and near wall regions. In central region, the current model estimates smaller absolutes of axial velocity than the results Yoshizawa model, and in near wall region, it estimates bigger absolutes of velocity. In figure 3, about circumferential velocity distribution, differences between the current model and the Yoshizawa model are seen only in near wall region at both sections. In this situation, current model estimates bigger absolutes of velocity than the results of Yoshizawa model.

Figure 4 shows circumferentially averaged distributions of isotropic eddy viscosity which are calculated by current model and Yoshizawa model at sections of 14 R_0 and 17.8 R_0. In both sections, absolute value of current model is smaller than that of Yoshizawa model at small region near center, this relation turn over in intermediate region, and the value is smaller than that of Yoshizawa model again at near wall. Also, the absolute values of both models have increasing tendency depending on

distance from the inlet.

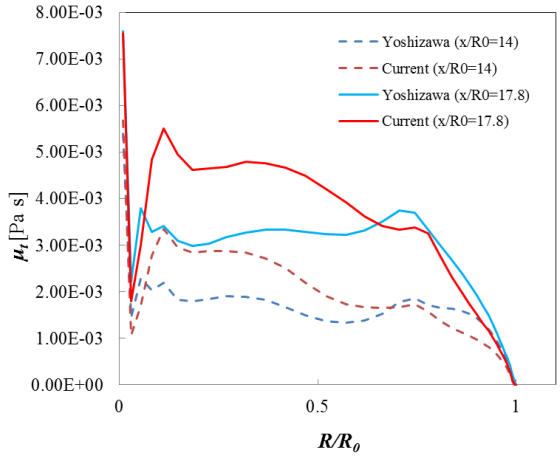

Figure 4: Isotropic eddy viscosity distribution

Figure 5 shows six components of turbulent stress along "y" axis of Cartesian coordinate at section $14\,R_0$. These components aren't averaged circumferentially, and these are described as below: R_{xx}, R_{xy}, R_{xz}, R_{yy}, R_{yz} and R_{zz}. In this situation, "x", "y" and "z" axis of Cartesian coordinate are equivalent to "axial", "radial" and "circumferential" direction, respectively. Display rule of stress tensor is canonical that first of two index indicates direction of normal vector of face applying stress, and second index indicates direction of stress.

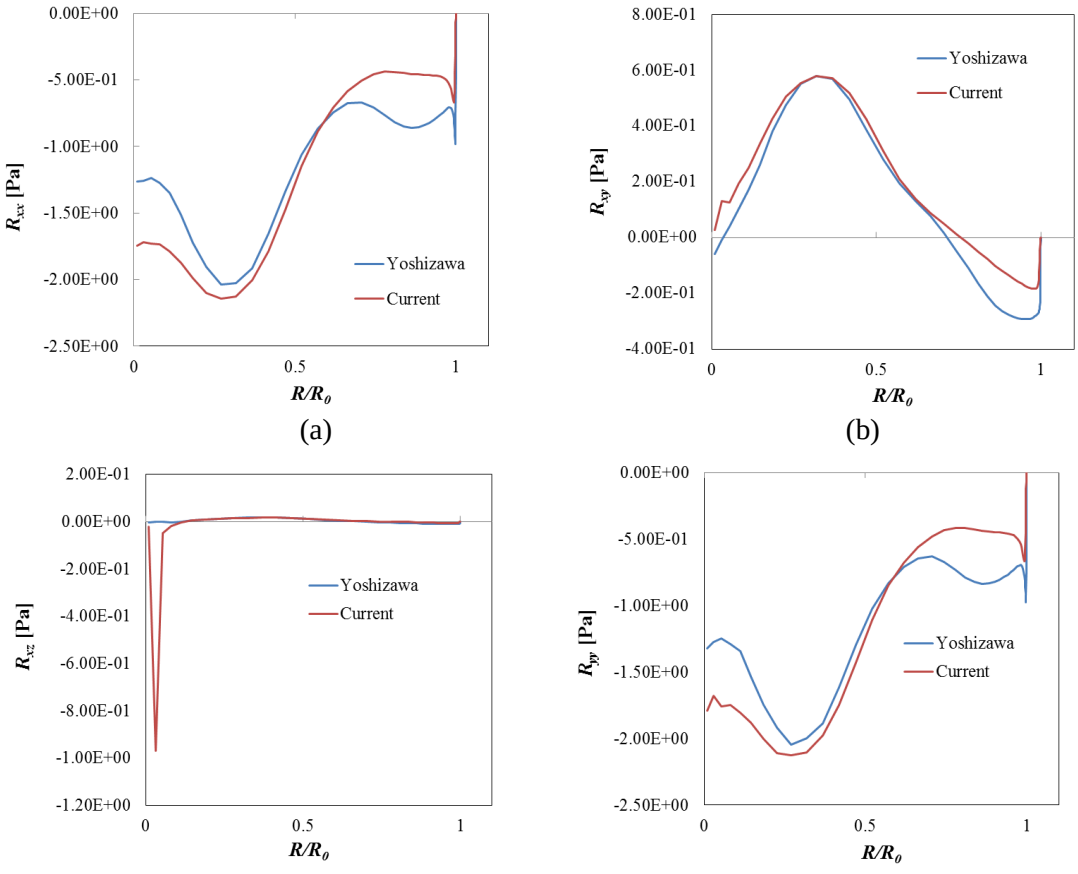

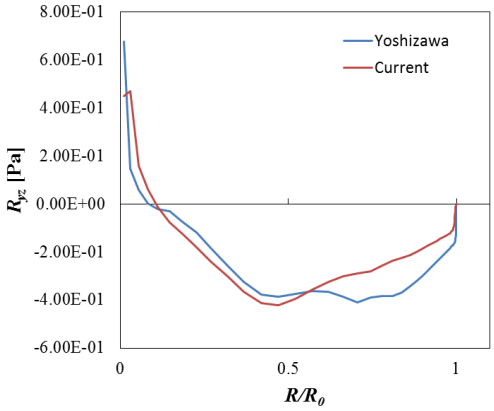

(e)

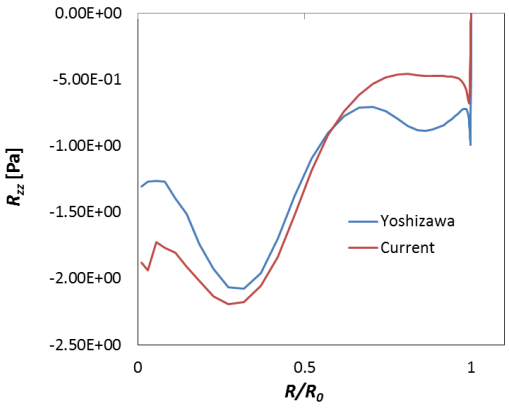

(f)

Figure 5: Components of turbulent stress

From figure 5 (a) and (c) (R_{xx} and R_{xz}), it can be seen that the absolute value of turbulent stress by current model is bigger than that of Yoshizawa model in central region. Hence, "x" directional momentum decrease as compared to the result of Yoshizawa model, and the difference of axial velocity distribution arises as central region of figure 2. Also, from figure 5 (a) and (b) (R_{xx} and R_{xy}), it can be seen that the absolute value of turbulent stress by current model is smaller than that of Yoshizawa model in near wall region. Hence, "x" directional momentum doesn't decrease as compared to the result of Yoshizawa model, and the axial velocity distribution is maintained as near wall region of figure 2. Additionally, from figure 5 (e) and (f) (R_{yz} and R_{zz}), it can be seen that the absolute value of turbulent stress by current model is smaller than that of Yoshizawa model in near wall region. Hence, "z" directional momentum doesn't decrease as compared to the result of Yoshizawa model, and the difference of circumferential velocity distribution arises as near wall region of figure 3.

Second, the simulation results for the experiment by Kito are shown. Figure 6 and Figure 7 indicate radial distribution of axial velocity and circumferential velocity, respectively, both of them are averaged circumferentially and are nondimensionalized. The means of lines and colors are same as figure 2 and figure 3, and the positions of measuring section are 24.6 R_0 and 38 R_0 from inlet.

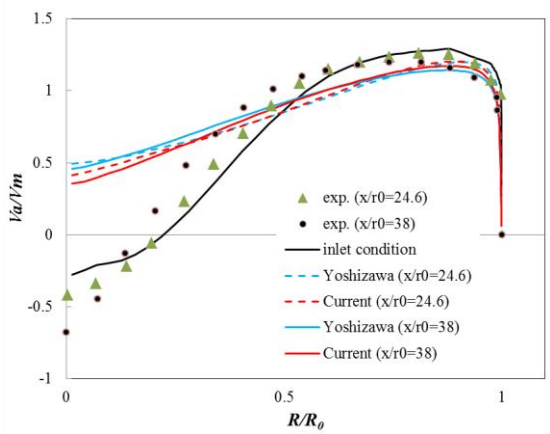

Figure 6: Axial velocity distributions

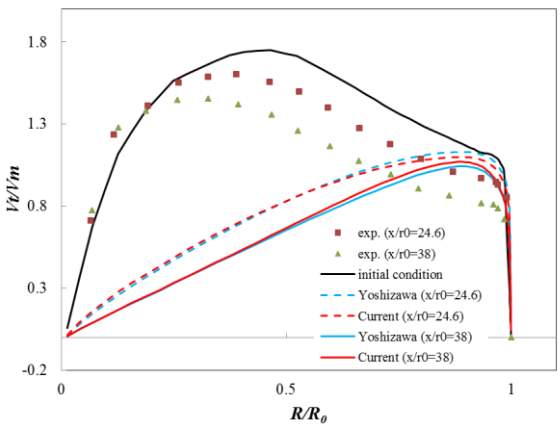

Figure 7: Circumferential velocity distributions

In figure 6 and 7, even distances from inlet to positions of measuring section are longer than the cases of Murakami, it can be seen that both of current model and Yoshizawa model can't simulate experimental results of Kito. Though, both distributions have trends similar to cases of Murakami.

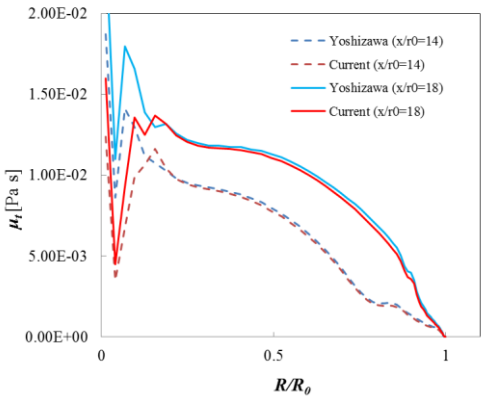

Figure 8: Isotropic eddy viscosity distribution

Figure 8 shows circumferentially averaged distributions of isotropic eddy viscosity which are calculated by current model and Yoshizawa model at sections of $14\,R_0$ and $18\,R_0$. Unlike simulation case for the experiment of Murakami, the value isn't changed by turbulence models except central region of pipe, and distributions in this region have same trend to simulation results for the case of Murakami. When figure 8 and figure 4 are compared, it can be seen that values of eddy viscosity in figure 8 is several times bigger than that of figure 8. Hence, it is thought that both models cannot simulate the experimental results due to defection of damping eddy viscosity.

7 Summary

In this study, Yoshizawa model is improved by adding nonlinear term of turbulent stress formulation of helicity model in order to append property of anisotropy to eddy viscosity. In the case of simulation for experiment of Murakami et al., which doesn't have reverse flow in central region, axial velocity distributions are slightly improved at central and near wall region, and absolute value of circumferential velocity become bigger than that of Yoshizawa model.

Meanwhile, in the case of simulation for experiment of Kito, which have strong reverse flow in central region, both Yoshizawa model and current model cannot achieve favorable results.

References

[1] Yoshizawa, A., et al., "Turbulent-viscosity modeling applicable to swirling flows, based on a composite time scale with mean-flow helicity partially incorporated", Journal of Turbulence.

[2] Murakami, M., et al., "An Experimental Study of Swirling Flow in Pipes", Transactions of the Japan Society of Mechanical Engineers. B, vol.41, No.346, pp.1793-1801, 1975.

[3] Motoe, M, et al.," Validation of Numerical Simulation of Swirling Turbulent Flow for Hybrid Rocket Research", AIAA 2011-560

[4] Yokoi, N., et al., "Three-Equation Turbulence Model with Coherent Structures Incorporated through the Helicity : Application to a Swirling Flow in a Straight Pipe", Transactions of the Japan Society of Mechanical Engineers. B, vol.58, No.553, pp.2714-2721, 1992.

[5] Shima, E., et al., "On New Simple Low-Dissipation Scheme of AUSM-Family for All Speeds", AIAA Paper 2009-0136

[6] Kito, O., "Experimental study of turbulent swirling flow in a straight pipe", Journal of Fluid Machanics, vol. 225, pp.445-479, 1991